Journal of Computational Physics **155,** 75–95 (1999)
Article ID jcph.1999.6330, available online at http://www.idealibrary.com on IDEAL®

A Shape Decomposition Technique in Electrical Impedance Tomography

David K. Han* and Andrea Prosperetti†

**Applied Physics Laboratory, The Johns Hopkins University, Laurel, Maryland 20723; †Department of Mechanical Engineering, The Johns Hopkins University, Baltimore, Maryland 21218 and Department of Applied Physics, Twente Institute of Mechanics, and Burgerscentrum, University of Twente, AE 7500 Enschede, The Netherlands*
E-mail: David.Han@jhuapl.edu, prosperetti@jhu.edu

Received December 28, 1998; revised June 15, 1999

Consider a two-dimensional domain containing a medium with unit electrical conductivity and one or more non-conducting objects. The problem considered here is that of identifying shape and position of the objects on the sole basis of measurements on the external boundary of the domain. An iterative technique is presented in which a sequence of solutions of the direct problem is generated by a boundary element method on the basis of assumed positions and shapes of the objects. The key new aspect of the approach is that the boundary of each object is represented in terms of Fourier coefficients rather than a point-wise discretization. These Fourier coefficients generate the fundamental "shapes" mentioned in the title in terms of which the object shape is decomposed. The iterative procedure consists in the successive updating of the Fourier coefficients at every step by means of the Levenberg–Marquardt algorithm. It is shown that the Fourier decomposition—which, essentially, amounts to a form of image compression—enables the algorithm to image the embedded objects with unprecedented accuracy and clarity. In a separate paper, the method has also been extended to three dimensions with equally good results.

Key Words: electrical impedance tomography; inverse problems; image compression.

1. INTRODUCTION

The general problem of electrical impedance tomography consists in the reconstruction of an unknown impedance distribution in a spatial region on the basis of measurements on the boundary. The technique, originally developed for biomedical and geological applications, uses an array of electrodes placed on the boundary of the domain of interest (see, e.g., Refs. [1, 2] for recent reviews). A sequence of prescribed voltages (or currents) is applied

0021-9991/99 $30.00

to these electrodes, and the resulting currents (or voltages) are measured. The problem that arises in this way falls in the category of so-called inverse problems as the solution sought is not the calculation of currents (or voltages) given voltages (or currents) and the parameters of the domain—as in the direct problem—but the characterization of the domain itself. It is well known that problems of this type are ill posed so that small amounts of measurement noise are sufficient to render a faithful resolution impossible. It is therefore essential to stabilize the solution against the instability resulting from noisy data.

In the present paper we address a special class of problems of this type, in which the region of interest is two-dimensional and the unknown electrical conductivity has a constant value of unity except in the interior of one or more objects where it vanishes. We consider measurements at very low frequency so that the impedance is purely real and reduces to the resistivity. In Ref. [3] some encouraging preliminary results in which the present method is extended to three dimensions were shown.

Situations of the type we study may arise for example in two-phase flow, where long bubbles rise in tubes in the so-called slug flow regime, the detection of buried cables, the imaging of bones or vessels in limbs, of lungs in the chest, non-destructive evaluation, and others.

In general, the approaches developed to date to determine an unknown impedance distribution fall into two classes. One is the so-called back-projection method, which is basically an adaptation of the technique developed for medical CAT-scans. Barber and Brown [4, 5] were the first to produce the image of a human forearm using this method, although the sharpness of the image was limited. Santosa and Vogelius [6] later improved the technique by using the conjugate residual method. Guardo *et al.* [7] also used the back-projection method in their study and gave an experimental demonstration in a three-dimensional case. So far, the back-projection method has been applied only to situations in which the conductivity contrast is small. It is not clear whether it can be extended to the problem considered here where, on the contrary, it is large.

The other approach, called "model based," consists in the generation of a sequence of solutions of the direct, or forward, problem, in which the currents (or voltages) predicted on the basis of an assumed impedance distribution are compared with those measured. At each step the assumed impedance distribution is refined in such a way as to decrease the mismatch between the forward solution and measurement (see, e.g., Refs. [1, 2, 8–11]). This is the path that we follow in the present paper. In our implementation we use the boundary integral method for the forward problem (see, e.g., Refs. [12, 13]), and the Levenberg–Marquardt algorithm (see, e.g., Ref. [14]) for the inverse problem. The key new feature that we introduce—and that results in a remarkable improvement over existing methods—is the description of the boundary of the objects in terms of a Fourier series, rather than a point-wise discretization. In this way, we are plagued far less than previous investigators by the instability of the solution with respect to measurement noise.

2. MATHEMATICAL MODEL

We consider a medium with uniform electric conductivity occupying a two-dimensional plane region Ω bounded externally by a circle $\mathcal{C}$ and internally by one or more curves Σ_j with $j = 1, 2, \ldots, m$. The electrical conductivity vanishes inside the internal boundaries. The objective of the tomographic reconstruction is to deduce the shape of the internal boundaries from measurements on the external boundary of Ω.

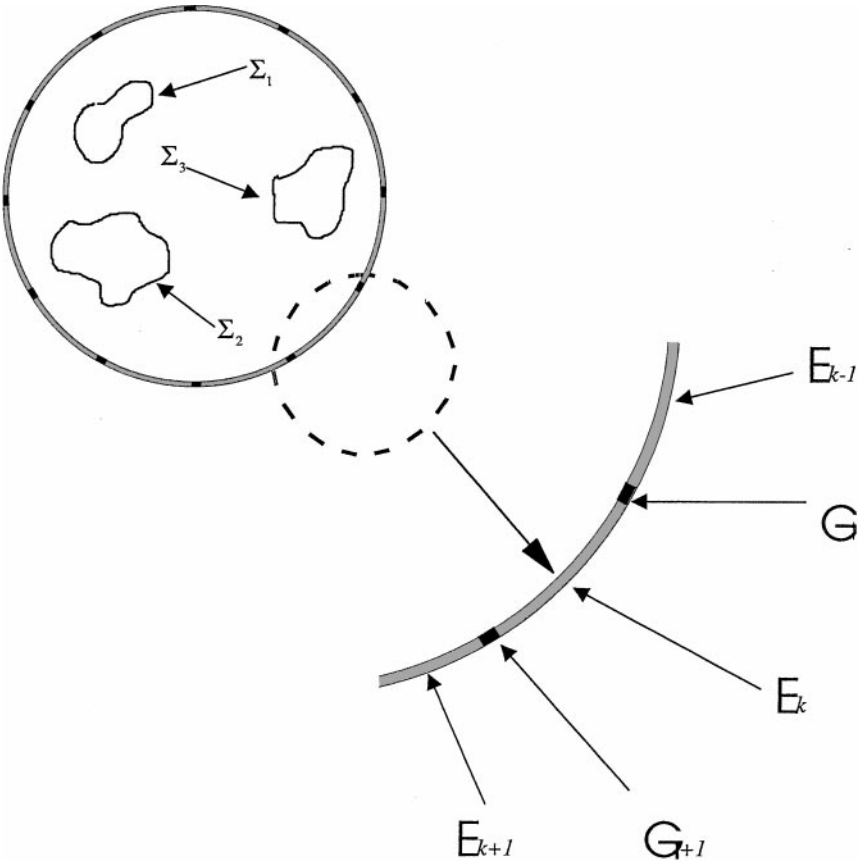

FIG. 1. Computational domain with 3 non-conducting objects. The inset shows the boundary with gaps and electrodes.

This external boundary consists of a number of equal, evenly spaced, perfectly conducting electrodes $\mathcal{E}_k$ separated by perfectly insulating gaps $\mathcal{G}_l$ as shown in Fig. 1. In practice, of course, there will be some contact resistance that would, however, be highly dependent on the particular experimental set-up and conditions [15, 16]. Since this effect cannot be meaningfully modeled in general terms, we do not attempt to include it although it may, in practice, have quantitatively significant effects.

In principle the data needed for the tomographic image reconstruction can be acquired either by imposing a current pattern on the electrodes and measuring the resulting voltages or, reciprocally, by imposing voltages and measuring currents. The latter alternative leads to a somewhat simpler modeling as, in practice, electrodes consist of highly conductive material throughout which the voltage can be assumed to be spatially uniform. When the total current into an electrode is specified, on the other hand, the current density is not uniform but needs to be determined from the solution of a boundary value problem. For this reason, for the sake of simplicity, we consider here a situation in which voltages are prescribed and currents measured.

As in other model-based algorithms, our method consists of the solution of a sequence of forward problems in which a better and better approximation to the internal boundaries Σ_j is progressively constructed.

The mathematical formulation of the forward problem is the following. The electric potential V inside the region Ω satisfies Laplace's equation

$$\nabla^2 V = 0, \tag{1}$$

subject to the condition of an imposed voltage V_k on the kth electrode $\mathcal{E}_k$ and of zero current in the lth gap $\mathcal{G}_l$. Mathematically, this latter condition is expressed by

$$\mathbf{n} \cdot \boldsymbol{\nabla} V = 0 \qquad \text{over } \mathcal{G}_l. \tag{2}$$

The same condition applies at the inner boundaries Σ_j. Here and in the following we set the electrical conductivity of the material to 1 for convenience.

The normal current density $n \cdot \boldsymbol{\nabla} V$ on the kth electrode and the total current I_k through it are related by

$$I_k = \int_{\mathcal{E}_k} \mathbf{n} \cdot \boldsymbol{\nabla} V \, d\mathcal{E}_k. \tag{3}$$

A comparison of these calculated currents with the measured ones gives a measure of the accuracy of the reconstruction and a means to refine it.

The ill-posed nature of tomographic reconstruction manifests itself in an ill-conditioning of the matrix of the system the solution of which gives the parameters defining the image. In the past the difficulty due to this ill-conditioning has been mitigated by the use of techniques such as the singular value decomposition, but at the expense of a significant sacrifice in image quality (see, e.g., Ref. [17]). The degree of ill-conditioning grows as the number of unknowns used to parameterize the image is increased for a given number of measurements.

This remark suggests that a desirable feature of an inversion method would be the use of a description of the object in terms of a number of parameters as small as possible. From this perspective it is clear that a point-wise description of the object boundaries, such as the one used, for example, by Murai and Kagawa [18], is rather inefficient. For example, 4 points (i.e., 8 parameters) can only approximate a quadrilateral. A more complex shape would require a significantly larger number of parameters even for a very coarse representation.

We take a different approach, namely we try to reduce the number of parameters necessary for an acceptable approximation of the image by superposing fundamental shapes, each one characterized by a small number of parameters, whence the denomination "shape decomposition" of the present technique. One may interpret this idea as attempting to reconstruct a compressed version of the image of the original object. Such an approach is particularly valuable when some general information as to the general shape of the objects is available a priori. For example, circles can be described in terms of 3 parameters only, the position of the center, and the radius.

While there is of course a great latitude in the choice of the fundamental shapes, here we use, for each object, a Fourier decomposition of the type

$$|\mathbf{x} - \mathbf{x}_C| = \frac{1}{2} A_0 + \sum_{k=2}^{\infty} (A_k \cos k\theta + B_k \sin k\theta). \tag{4}$$

Here $\mathbf{x}_C \equiv (x_C, y_C)$ is the centroid of the object defined so that the term $k = 1$ is not present

in the expansion (4), i.e.,

$$\int_0^{2\pi} |\mathbf{x} - \mathbf{x}_C| \sin\theta \, d\theta = 0, \qquad \int_0^{2\pi} |\mathbf{x} - \mathbf{x}_C| \cos\theta \, d\theta = 0. \tag{5}$$

For a smooth contour, the series (4) converges faster than any power of $1/n$ and one may therefore expect that a small number of terms would be sufficient for an acceptable reconstruction.

The angle θ is measured from an arbitrary direction, that we take as the x-axis of a plane Cartesian coordinate system. In practice, of course, the series (4) is truncated to a finite number of modes $k_{max} = N$, after which the problem of image reconstruction is reduced to the calculation of the $2N - 1$ Fourier coefficients A_0, A_k, B_k, $k = 2, 3, \ldots, N$, and of the two coordinate (x_C, y_C) of the object centroid. The total number of unknowns is therefore $2N + 1$ per object; in a sense N can thus be thought of as a regularization parameter for the present method.

Clearly, the expansion (4) is only valid for shapes such that all rays issuing from $\mathbf{x}_C$ intersect the boundary of the object at one point only. This restriction can be alleviated in several ways. For example, one might use simultaneously more than one Fourier expansion centered at different points and suitably matched. Another possibility might be the use of a normalized arc length in place of the polar angle θ. Since we have not explored any of these alternatives yet, in this paper we shall only consider shapes that can be represented in the form (4).

3. NUMERICAL ASPECTS

It will be recalled that in the class of problems considered here the objects to be imaged have zero conductivity. This circumstance can be exploited to improve the tomographic reconstruction. In the first place, one can use a boundary integral method for the calculation of V according to (see, e.g., Refs. [12, 13])

$$V(\mathbf{x}) = \frac{1}{2\pi} \int \left(V(\mathbf{x}') \frac{\partial}{\partial n'} \log|\mathbf{x} - \mathbf{x}'| - \log|\mathbf{x} - \mathbf{x}'| \frac{\partial V}{\partial n'} \right) dl', \tag{6}$$

where the integral is over the entire boundary of the problem, i.e., the electrodes, the insulating gaps, and the interior object(s); the factor 2 in the denominator is because the field point $\mathbf{x}$ is on the boundary. This possibility is particularly advantageous here in view of the fact that only the normal gradient of V on the boundary is required in the present problem for the evaluation of (3). With a finite-element approach, the entire domain would have to be discretized and resolution and quality of the reconstructed image would strongly depend on the particular discretization used, particularly in the neighborhood of the objects.

In the numerical examples discussed below we assume that the electrode-to-gap area (or better, in two dimensions, arc length) ratio is 10 to 1 (Fig. 1). The number of nodes used for the electrodes and the gaps was progressively increased until the values of the currents stabilized to within 0.02%. Typically 29 and 17 nodes for each electrode and gap, respectively, were required. The nodes were denser near the edge of the electrodes to better resolve the square-root singularity of the current density there; 60 nodes were used for the boundary of the interior object, which tests proved to be sufficient for good accuracy. These nodes were equally spaced in the angular direction. In the implementation of the boundary

integral method we use cubic splines to describe the boundaries and a linear interpolation for V over each boundary element. Gaussian integration was used with 6 nodes on each element.

We made no attempt to optimize the boundary integral calculation. For instance, a parameterization of V that were to explicitly account for the square-root singularity at the electrode edges could reduce the number of nodes without sacrificing accuracy. On the other hand, it is likely that such an approach would have to be modified for example in the presence of a model for the contact resistance. We feel that this and other aspects of a similar nature are peripheral to the main point of this paper which is the introduction of the shape decomposition idea.

For the reasons discussed in the next section, the reconstruction procedure begins with a search for the circle(s) that best approximates the target. For each estimate of the target, the $\frac{1}{2}N(N-1)$ currents that are available with N electrodes are calculated from (3) and compared with the "measured" currents (i.e., the numerically generate pseudo-data). The Levenberg–Marquardt algorithm [14] is used to progressively refine the parameter values. This part of the procedure is very rapid as it only involves three parameters and is arrested when the relative difference between current values evaluated in two successive iterations falls below 10^{-4}. When this criterion is satisfied, a search for all the parameters included in the final search is started, but with a lower spatial discretization (11 nodes on the electrodes and 3 in the gaps). This procedure is arrested when a convergence criterion of 10^{-4} is met. Finally, a full search with the same number of nodes used for the generation of the pseudo-data is carried out and terminated as before with a convergence criterion of 10^{-4}–10^{-5}. In general it was found that, at the termination of the iteration procedure, the residual was of the order of 10^{-4}–10^{-5} times the initial value.

The computational time for the examplesthat follow on an SGI Octane workstation varied from a few minutes to several hours in the cases with the largest number (24) of electrodes.

4. RESULTS

In order to test the proposed method, in this paper we use "pseudo-data" generated from the solution of the forward problem with a given object shape. The Fourier coefficients used to parameterize the object are the "target" values that the inversion algorithm must reconstruct.

It must be recognized that, although this is a common procedure, the data are not "exact" and, in a sense, the numerical error introduces an uncontrolled regularization. Thus, in principle, one might even worry that an apparent ability to reconstruct the object might be fortuitous. In this connection we may note that, first, the pseudo-data that we use are essentially converged and, therefore, numerically indistinguishable from a hypothetical exact solution; second, the present method seems to work well even in the presence of noise (see below) and, third, satisfactory results are consistently recovered varying the number of Fourier components, electrodes, and objects. Hence we believe that the results that we describe furnish a sufficiently stringent test of the ability of the present shape decomposition algorithm.

We have tested the method both with objects that can be represented exactly by the superposition of a finite number of Fourier modes, which we call *Fourier objects*, and with objects for which any finite Fourier representation is only an approximation of the real shape, *non-Fourier objects*. Although perhaps not very realistic, Fourier objects are useful as their exact reconstruction by the algorithm is, in principle, possible. Any error can therefore by imputed to the method itself rather than to the accuracy with which a truncated Fourier

series represents the actual shape. Thus Fourier objects enable us to get a good assessment of the properties of the algorithm, e.g., its sensitivity to factors such as shape complexity, number of electrodes used, and object location.

4.1. *Fourier Objects*

For Fourier objects, one can envisage situations where the number of Fourier modes is known a priori or not. The former case is obviously simpler and we begin by one such example.

We consider an object generated with 8 Fourier modes, i.e., a total of 17 parameters, with $x_C = y_C = 0$. The inversion algorithm based on an 18-electrode system, searched for all the 17 parameters at the same time and the starting guess was a circle of radius 0.3 at the center of the domain. The solid line in Fig. 2 shows the object and the dashed line the image reconstructed by the inversion algorithm when the convergence criterion was satisfied after 18 steps. Table I gives the values of the exact Fourier amplitudes, the initial guess, and the final converged values (column 4). It can be seen that the algorithm performed well in this case.

It was found that when the procedure was applied to the same object displaced from the center of the domain, the accuracy of the reconstruction was affected by the position of the initial circle. A considerable improvement of the method's performance was achieved by adopting a different, more robust strategy that might be termed "deferred search": a preliminary search is conducted for the center and radius of an approximating circle and, once these parameters have been estimated, the search for the complete parameter set is turned on as described at the end of the previous section. Numerically, this procedure can be interpreted as a pre-conditioning of the iteration operator. With this strategy, excellent results were obtained irrespective of the location of the initial circle as shown in columns 5 and 6 of Table I that correspond to the same object of Fig. 2 centered at $(-0.2, 0)$ and $(-0.39, 0)$, respectively. A total of 26 and 29 iterations were required, respectively, starting from the domain's center; about 5 iterations were necessary to find the approximating circle. This same strategy was used for all the examples that follow.

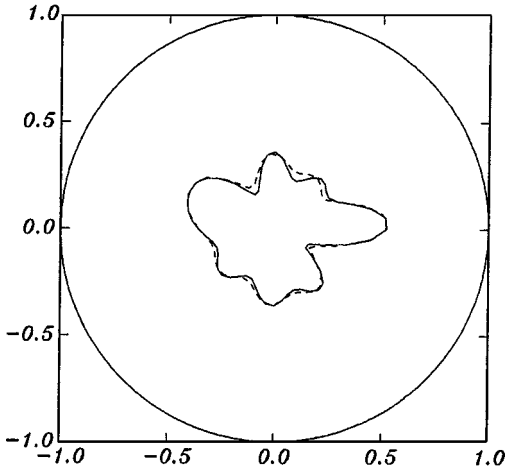

FIG. 2. Reconstruction on the basis of an 18-electrode system (dashed line) of an object generated with 8 Fourier modes (solid line). See Table I, column 4, for numerical values.

TABLE I

Exact Values, Initial Guesses, and Computed Results for the Object of Fig. 2 Centered at (0., 0.) (Column 4), (−0.2, 0) (Column 5), and (−0.39, 0.) (Last Column)

Parameter	Exact value	Initial guess	Calculated value (−0.0015, 0.0027)	Calculated value (−0.1997, 0.0007)	Calculated value (−0.3887, 0.0004)
A_0	0.3200	0.3000	0.3269	0.3262	0.3249
A_2	0.0400	0.0	0.0349	0.0365	0.0381
B_2	0.0	0.0	−0.0038	−0.0033	−0.0030
A_3	0.0	0.0	0.0031	0.0022	0.0015
B_3	0.0400	0.0	0.0330	0.0335	0.0343
A_4	0.0400	0.0	0.0421	0.0412	0.0408
B_4	0.0	0.0	−0.0030	−0.0043	−0.0041
A_5	0.0400	0.0	0.0420	0.0410	0.0406
B_5	0.0400	0.0	0.0329	0.0353	0.0365
A_6	0.0	0.0	0.0080	0.0056	0.0029
B_6	0.0	0.0	0.0014	0.0010	0.0013
A_7	0.0400	0.0	0.0382	0.0366	0.0366
B_7	0.0	0.0	0.0032	0.0034	0.0036
A_8	0.0400	0.0	0.0286	0.0315	0.0341
B_8	0.0	0.0	0.0009	0.0038	0.0030

Note. The calculated coordinates of the object center are shown at the top of the last 3 columns.

We now consider, again with 18 electrodes, two cases in which the number of parameters searched is not the same as that used to generate the object. In the first example, the number of parameters searched is smaller. In this case, one may expect that the higher-frequency components of the true shape act as noise contaminating the data presented to the inversion algorithm. The first panel of Fig. 3 shows an object centered at the origin and generated with 6 Fourier components (solid line) and its reconstructed image with only 5 Fourier components after 42 iterations (dashed line). The reconstructed image is clearly an approximation of the true image. The values of the reconstructed Fourier parameters for this case are shown in the fourth column of Table II. From these numerical results, we see that the approximation is acceptable in spite of the unavoidable error.

For the same object, we next allowed 7 Fourier modes in the image, i.e., one more than those necessary for an exact reconstruction. The results of the reconstruction after 41 iterations are shown in the second panel of Fig. 3 and the corresponding numerical values are given in the last column of Table II. The inversion algorithm was evidently successful in this case.

These results illustrate the ability of the inversion algorithm to reconstruct Fourier objects even when there are uncertainties in the number of modes used to generate them.

4.2. *Non-Fourier Objects*

The next set of trials involved image reconstruction of objects with shapes that cannot be described exactly by a small number of Fourier components. To present a challenge to the reconstruction algorithm we chose objects with fairly sharp corners. Even though, being generated with cubic splines, these figures do not possess actual sharp corners that would result in a k^{-2} decay of the Fourier coefficients, traces of the slow convergence of the Fourier representation may still be expected to remain. This circumstance renders a relatively large

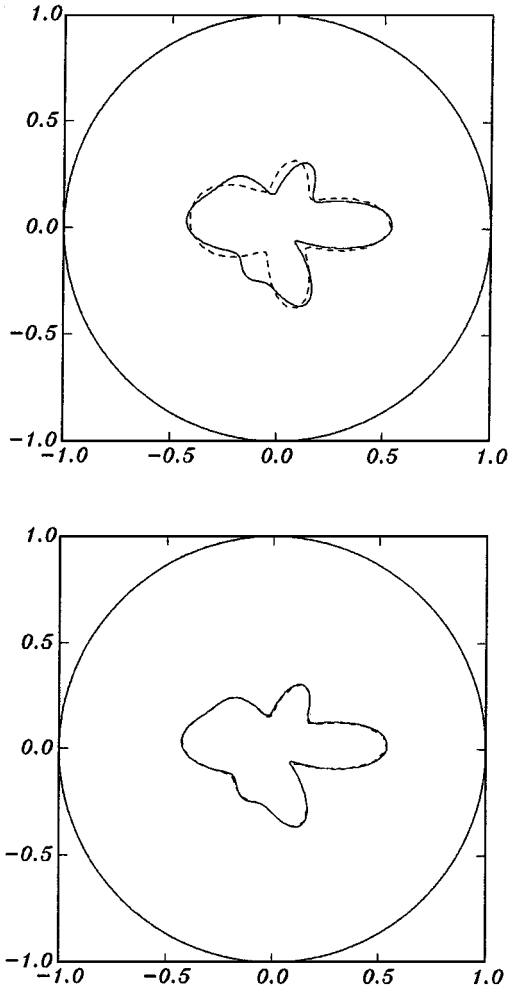

FIG. 3. An object generated with 6 Fourier modes (solid lines) is reconstructed (dashed lines) searching for 5 modes (upper panel) and 7 modes (lower panel) on the basis of an 18-electrode system. For numerical values see Table II.

number of modes necessary for an accurate reconstruction and, therefore, such objects represent a more stringent test for the inversion than those considered previously.

The first example is a pentagon-shaped object centered at (0.259, 0.259). Figures 4a and 4b show the results of two reconstruction attempts based on 5 (12 iterations, first panel) and 6 (14 iterations, second panel) modes, respectively, in both cases on the basis of data corresponding to 16 electrodes. The true object is shown by the solid line and the final converged images by dashed lines. There is little difference between the two reconstructions.

Next a rotated L-shape was reconstructed searching for 5 and 6 Fourier modes, in both cases with the same convergence criteria. Since this case is a more difficult one, we used simulated data with a 24-electrode system. The converged images, obtained after 15 and 39 iterations, respectively, are shown in Fig. 5. Both searches captured the essence of the object features fairly successfully, but with varying degree of distortion. We also tried 7 Fourier modes, but without any significant improvement in the image quality.

TABLE II
Exact Values, Initial Guess, and Computed Results for the Object of Fig. 3 Constructed with 6 Fourier Modes

Parameter	Exact value (0, 0)	Initial guess (0, 0)	Calculated value (−0.0238, 0.0102)	Calculated value (−0.0002, −0.0028)
A_0	0.3000	0.3000	0.2966	0.3003
A_2	0.0600	0.0	0.0761	0.0613
B_2	0.0	0.0	−0.0122	−0.0020
A_3	0.0	0.0	−0.0153	−0.0002
B_3	0.0600	0.0	0.0337	0.0592
A_4	0.0600	0.0	0.1001	0.0575
B_4	0.0	0.0	0.0033	0.0007
A_5	0.0600	0.0	0.0539	0.0614
B_5	0.0	0.0	−0.0056	0.0003
A_6	0.0600	0.0	0.0	0.0607
B_6	0.0	0.0	0.0	0.0015
A_7	0.0	0.0	0.0	0.0001
B_7	0.0	0.0	0.0	0.0046

Note. The calculated coefficients with a 5- and a 7-mode reconstruction are shown in the 2 last columns. Since 5 modes are insufficient for an exact reconstruction of the object, the corresponding results show an appreciable error.

4.3. *Noisy Data*

In the examples studied so far the objects were reconstructed from the simulated data of the forward solution algorithm without any added noise. In view of the ill-conditioning of the inverse problem, it is crucial to test whether the inversion algorithm is robust enough to tolerate noise in the data. It is also interesting to explore whether the performance of the method in the presence of noise can be improved by increasing the number of electrodes. Another parameter that affects the quality of the reconstruction is the number of Fourier modes kept in the search. Again, it is interesting to explore the robustness of the method as this parameter is varied in the presence of noise.

To test the stability of the algorithm with respect to errors in the data we generated artificial "noise" by introducing a random perturbation. As before, the data are simulated by solving the forward problem numerically and the perturbation is introduced according to the rule

$$\mathbf{P}' = \mathbf{P} + \epsilon r \|\mathbf{P}\|, \tag{7}$$

where r is a random number (different for each component of $\mathbf{P}$) with $-0.5 \le r \le 0.5$ and ϵ is a parameter quantifying the noise level. The elements of the vector $\mathbf{P}$ are the simulated electrode current data, the elements of $\mathbf{P}'$ are the corresponding "noisy" data, and $\|\mathbf{P}\|$ is the maximum norm. We consider $\epsilon = 1\%$ and 2%, which is of the order usually considered in the literature (see, e.g., Ref. [19]).

The first test was the reconstruction of the shape shown in Fig. 6, centered at (0, 0) and generated with 5 Fourier modes with various levels of noise. An 8-electrode system was simulated. The reconstructed images after contamination of the data by 1% and 2% noise levels are shown in Figs. 6a (15 iterations) and 6b (18 iterations). The reconstruction remains acceptable with a 2% noise level. We found that if the noise level is raised to 5%, the image

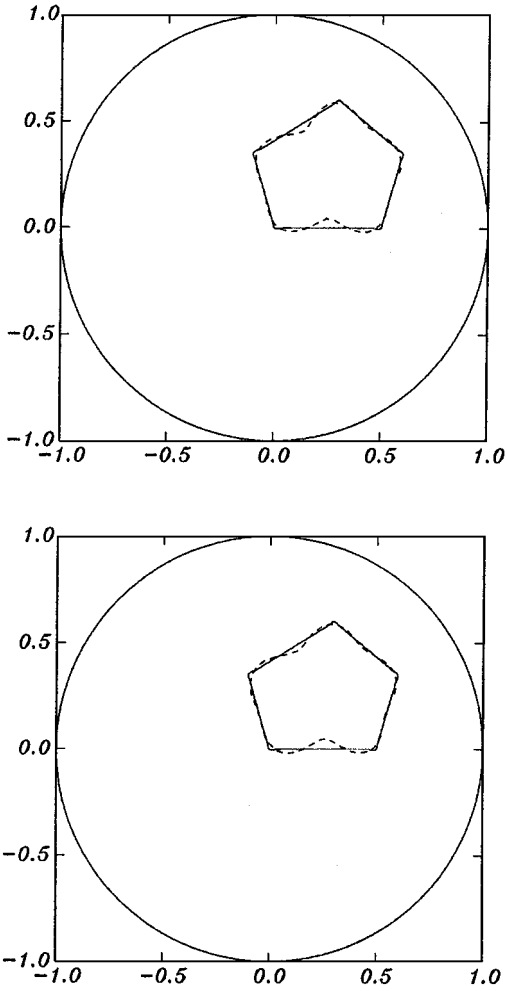

FIG. 4. A pentagon-shaped object reconstructed searching for 5 Fourier modes (upper panel) and 6 modes (lower panel) on the basis of a 16-electrode system.

quality is greatly degraded with the boundary notching inward toward the centroid as the higher frequency components grow large.

Similar results were found for the reconstruction of other types of images from noisy boundary measurement data. Figure 7 shows the reconstruction of a square object of side 0.5 centered at (0.25, 0.25) by a 16-electrode system at zero noise level (13 iterations, top panel) and at 1% and 2% noise level (14 and 19 iterations, respectively). If the noise level is further increased, the higher frequency components in the image grow and eventually dominate. Four Fourier modes were searched for in this case; the truncation of the exact shape to this small number of coefficients is evidently a form of regularization as mentioned before in Section 2.

Figure 8 shows the image of the square reconstructed with 4 (35 iterations), 6 (51 iterations), 7 (64 iterations), and 9 Fourier modes (57 iterations) with a noise level of 2% in the synthetic data generated by a 16-electrode system. As can be seen, the reconstruction becomes more and more unstable as the number of modes is increased.

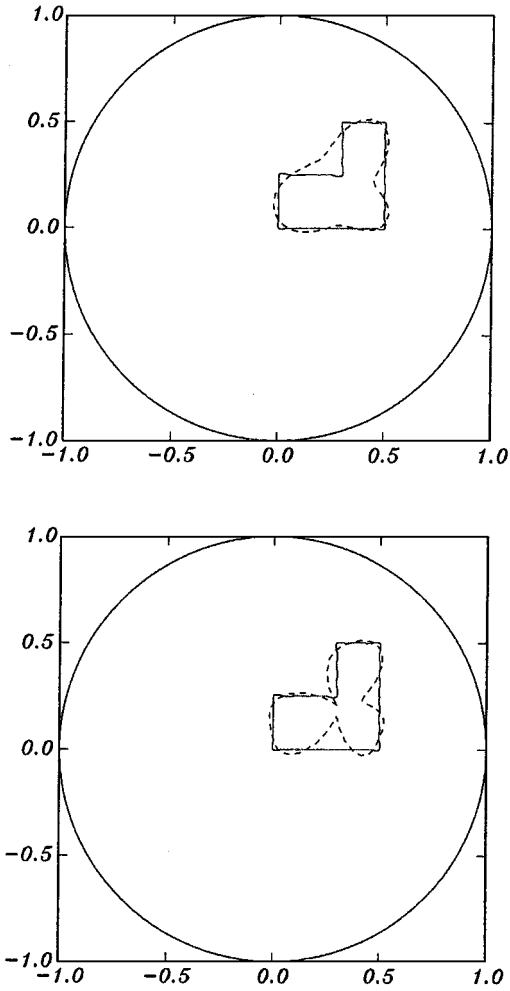

FIG. 5. An L-shaped object reconstructed searching for 5 (upper panel) and 6 (lower panel) Fourier modes with data simulated by a 24-electrode system.

The instability caused by noise in the data or a large number of parameters may be alleviated by utilizing a larger number of electrodes, i.e., by increasing the ratio of the number of measurements to that of unknowns. The number of distinct measurements obtainable with N electrodes is obviously the number of distinct pairs into which they can be grouped, i.e., $\frac{1}{2}N(N-1)$. Therefore, the number of distinct data increases quadratically with the number of electrodes although, beyond a certain point, the difference between the data produced by neighboring electrode pairs becomes too small to mitigate the ill-conditioning of the problem. Nevertheless we find that increasing the number of electrodes does help with image reconstruction in the presence of noise. Some examples are shown in Fig. 9 where the results of attempts at reconstruction of the square used before with 12, 16, and 24 electrodes are shown in the presence of 1% and 2% noise levels. For the 1% noise level (Figs. 9a to 9c) the number of iterations necessary for convergence was 20, 16, and 15, respectively. For a 2% noise level, convergence was not achieved for the 12- and 16-electrode systems (Figs. 9d, 9e), while it occurred after 16 iterations with 24 electrodes (Fig. 9f). In spite of some degree of degradation, the image produced by the 16-electrode system captured the key features

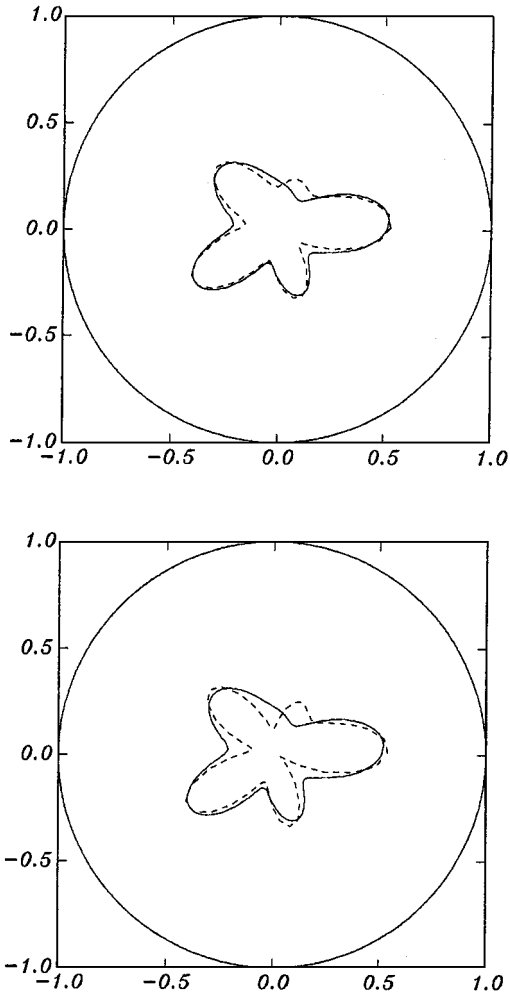

FIG. 6. Attempted reconstructions (dashed lines) of an object generated with 5 Fourier modes in the presence of 1% (top panel), and 2% (lower panel) noise.

of the object successfully at the 1% noise level. At 2%, however, the images reconstructed with fewer electrodes were strongly affected by the noise. Although in our experience the larger number of electrodes has consistently yielded better results, this conclusion is based on observations of a limited number of tests. Both theoretical and numerical investigations are needed to gain additional insight into this issue.

4.4. *Several Objects*

We now present results of a preliminary test of the performance of the inversion algorithm when more than one object is present.

The first case we consider has two Fourier objects. Figure 10 shows a sequence of intermediate images during the reconstruction process for non-noisy synthetic data generated by an 8-electrode system. In this case, the number of objects to be reconstructed was prescribed at the beginning of the inversion. Each object was generated with 3 Fourier modes, for a total number of 14 unknowns. This information about the number of parameters for each

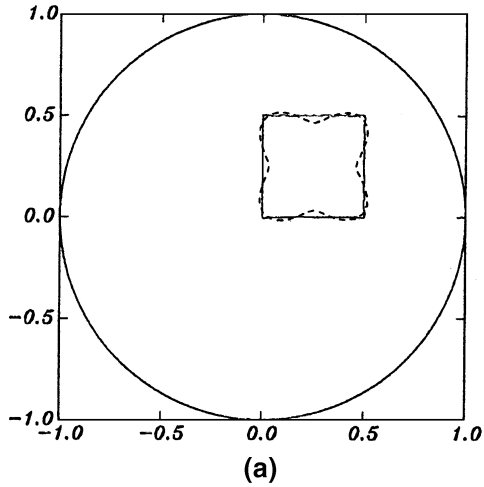

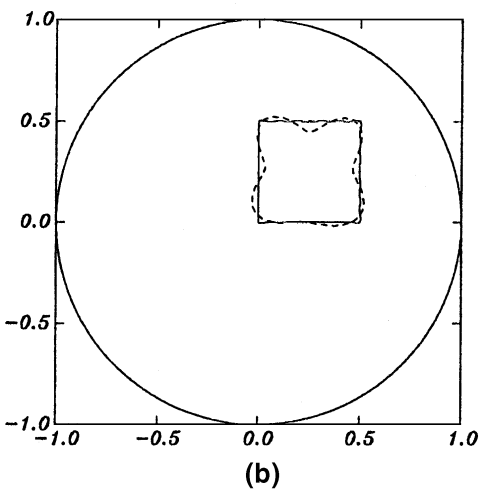

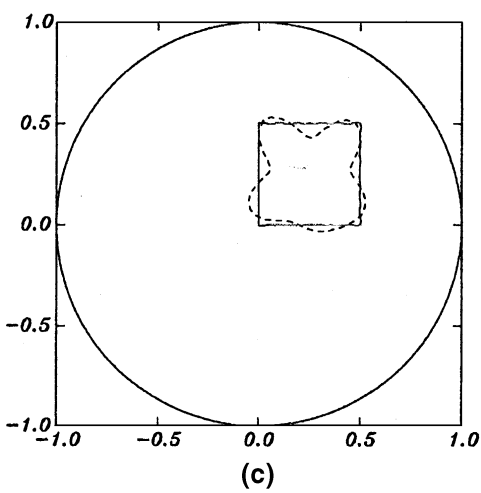

FIG. 7. Attempted reconstruction of a square with (a) no noise; (b) 1% noise; (c) 2% noise, all with data generated by a 12-electrode system searching for 4 Fourier modes.

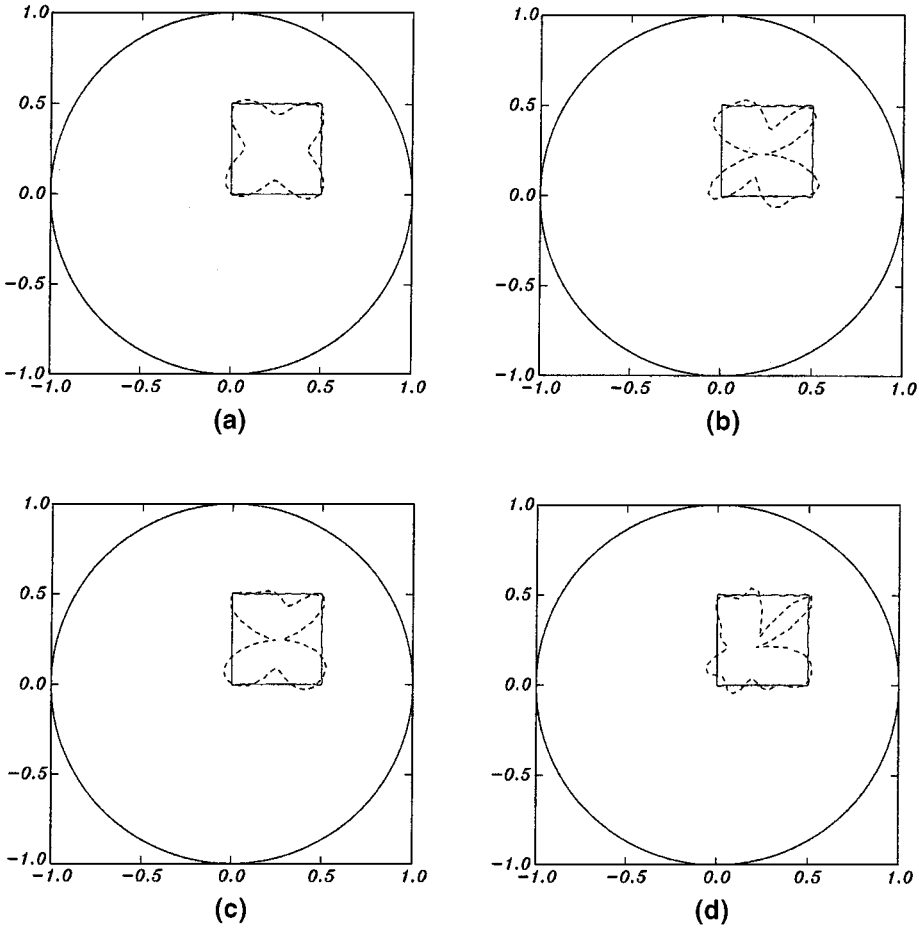

FIG. 8. Attempted reconstruction of the square of the previous figure in the presence of a 2% noise level searching for (a) 4 Fourier modes; (b) 6 modes; (c) 7 modes; (d) 9 modes; pseudo-data generated by a 16-electrode system.

object was also specified at the beginning of the calculation. After 13 iterations the inverse solution converged to the true image as shown in the last panel of Fig. 10.

In general, the number of objects present in the domain may be one of the unknowns of the problem. As an example of such a situation we consider the following test conducted without the deferred search strategy. The first panel of Fig. 11 shows the same square-shaped object used before together with an initial guess constituted by two circles. We expected that if one of the images converged to the true object, the other one would be forced to a small size to minimize the error. The data were generated from the simulation of a 24-electrode system with no noise contamination and 3 Fourier modes each were allowed in the reconstructed objects. The final panel of Fig. 11 shows the result after 50 iterations, at which point the results started fluctuating and the procedure was stopped. It is likely that this outcome was due to a loss of accuracy of the boundary integral calculation caused by the intersection of the boundaries. Nevertheless we show this result to demonstrate the tendency of the two objects to coalesce in these conditions in an effort to reproduce the target.

The deferred search strategy suggests a simple way to prevent such coalescence of boundaries. Instead of forcing the reconstruction to converge quickly, which causes the algorithm

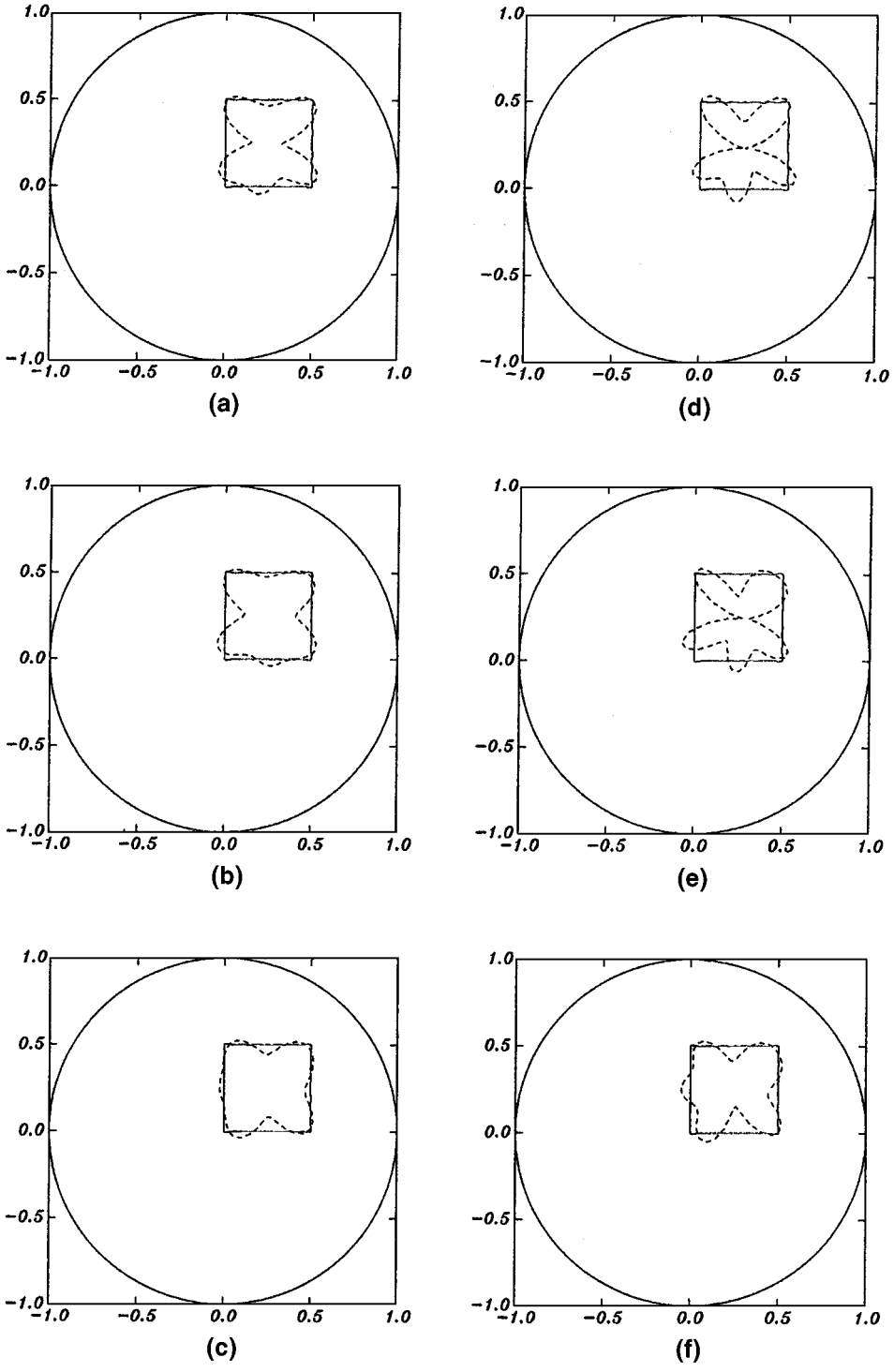

FIG. 9. Attempted reconstruction of the square of the previous figures in the presence of a 1% noise level (a)–(c), and a 2% noise level (d)–(f) with 12 electrodes (a), (d), 16 electrodes (b), (e), and 24 electrodes (c), (f).

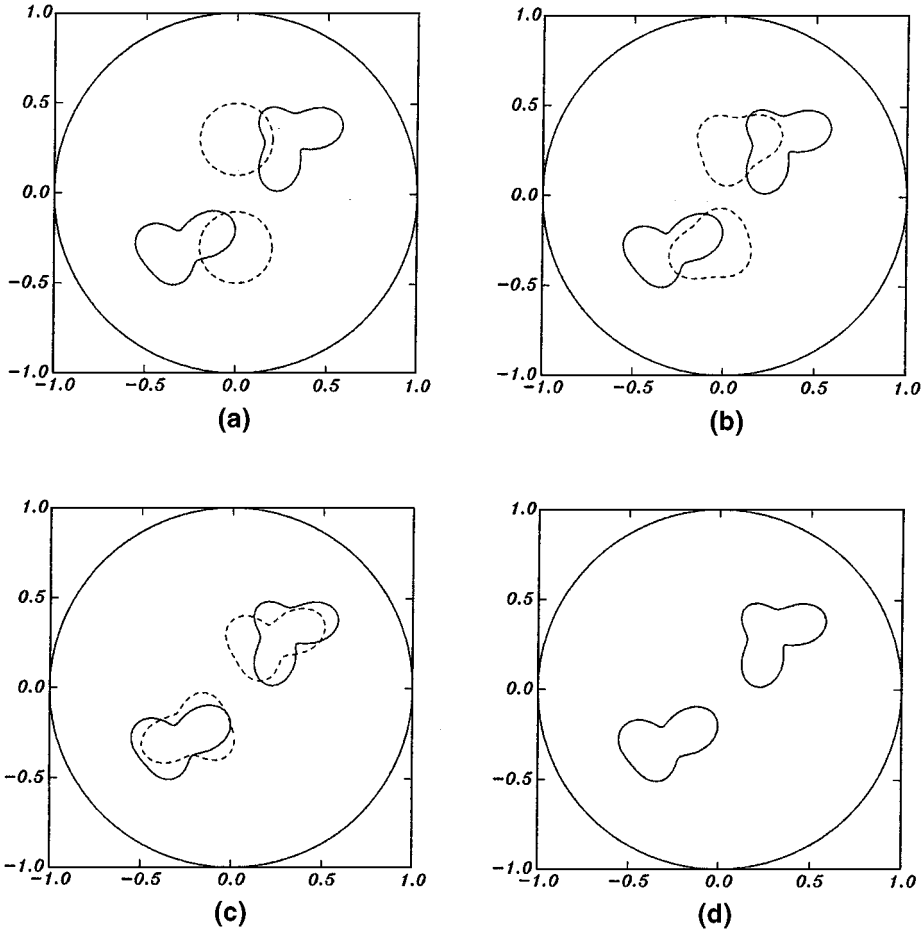

FIG. 10. Snapshots of the convergence history of a two-object reconstruction with no noise contamination; (a) initial guess; (b) first iteration; (c) second iteration; (d) converged results after 13 iterations. Pseudo-data generated by an 8-electrode system.

to try and fit the two images into a single object, one may first look just for the number of circles that minimizes the difference between true and inverted data.[1] This forces the inversion not to try to fit two deformed images onto a single object. After the number of objects to be reconstructed is determined in this way, the inversion can proceeded normally. A few snapshots of such a reconstruction sequence, based on a 12-electrode system, are shown in Fig. 12. This approach can be extended to the case of several objects. One would start with a certain number of circles as the initial guess. If this number is larger than that of the objects, one would progressively eliminate any circle whose radius becomes too small. If this does not happen, the initial number of circles should be increased until some are eliminated thus ensuring that the correct number of objects has been identified. The starting guess of the second phase of the solution would of course exploit the calculated information on the centroid location and approximate radius of each object. This knowledge of the

[1] Although one would expect the existence of such a minimum in many cases, it should be noted that no formal proof is available.

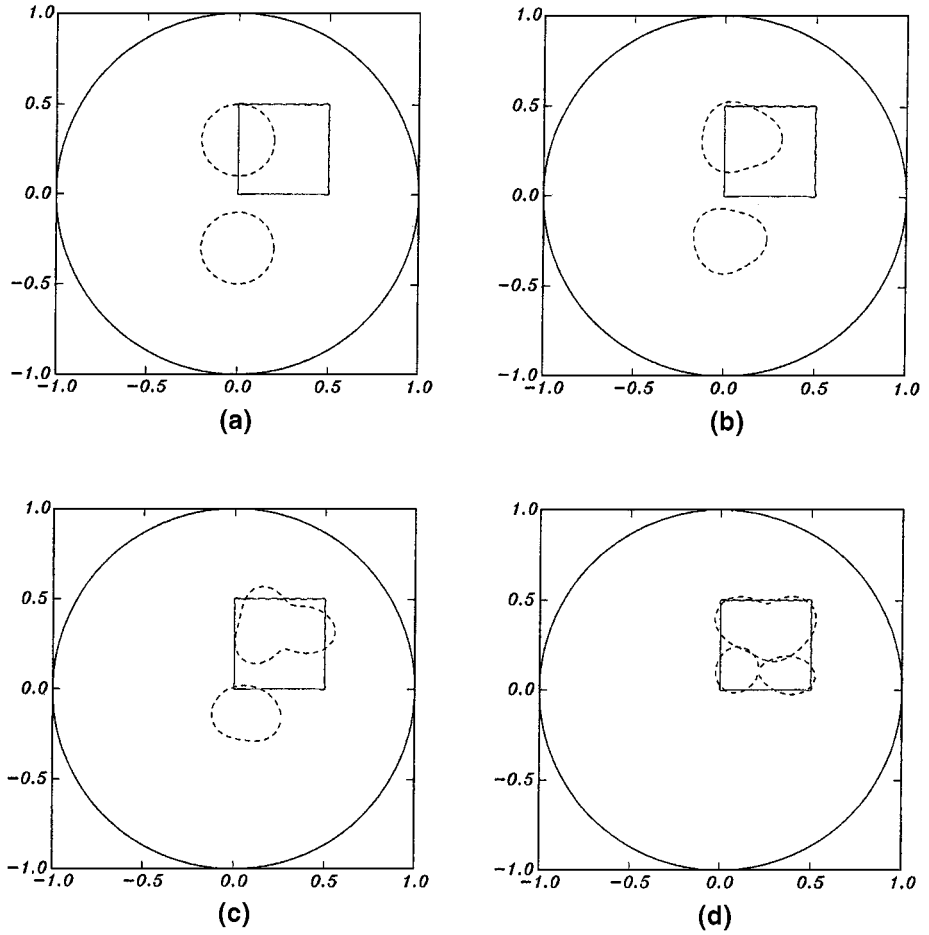

FIG. 11. Attempted reconstruction of the square of Fig. 7 searching for two objects; (a) initial guess; (b) first iteration; (c) second iteration; (d) after 50 iterations. Pseudo-data generated by a 24-electrode system with no noise contamination.

general location of the objects can be expected to help prevent the settling of the solution into a local minimum.

5. CONCLUSIONS AND COMMENTS

This paper has introduced a new approach to image reconstruction by electrical impedance tomography. By fitting the object by means of suitable "shapes"—as opposed to a discrete number of points—one can increase the resolution of the object to be reconstructed without a large increase in the number of parameters that need to be specified. As a consequence, the number of unknowns can be kept relatively small, and sensitivity to the inherent ill-posedness of the problem correspondingly reduced. The idea is to attempt the reconstruction of an effectively "compressed" image, i.e., one that can be approximated well with a small number of parameters. Alternatively, one may think of an object describable in terms of several different representations each one characterized by a number—usually infinite—of "degrees of freedom." Clearly, it is advantageous to attempt the reconstruction of the object in terms of the representation that, in a suitable sense, converges the fastest.

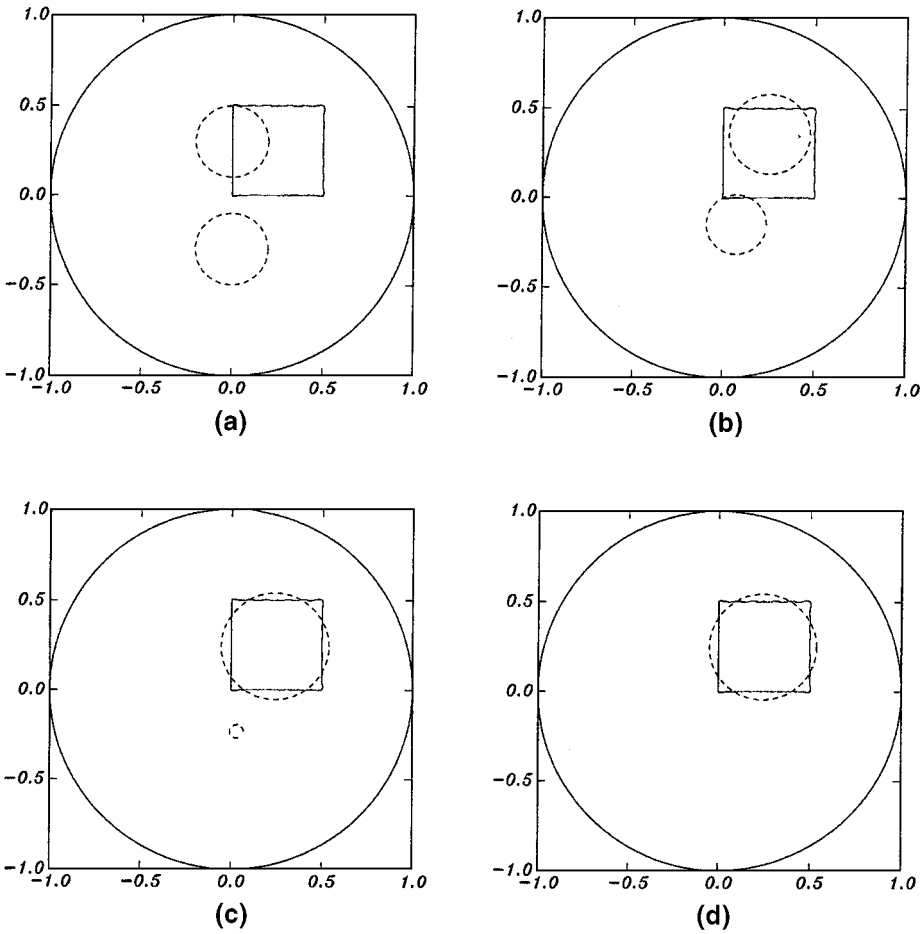

FIG. 12. Attempted reconstruction of the square of the previous figure in terms of two circles; (a) initial guess; (b) second iteration; (c) fourth iteration; (d) converged result after 9 iterations. Pseudo-data generated by a 12-electrode system with no noise contamination.

In this study we have represented the object by means of a truncated Fourier series as it is well known that the Fourier coefficients of a smooth function converge faster than algebraically. Clearly the essence of the idea introduced here can be implemented in a variety of ways. The present study was only meant to introduce the concept and demonstrate its performance in a number of examples. In conclusion, we indicate a number of points for further research:

1. In order to start the search from an initial guess relatively close to the solution it is useful to adopt the strategy of "deferred search": a preliminary low-resolution search in terms of circles or other simple shapes is conducted to estimate the number, position, and general size of the objects. The final search can then be based on these preliminary results with an increase in speed of convergence. This approach may be interpreted as a preconditioning of the operator and alternative, more efficient strategies of this type may exist.

2. As expected, the inversion algorithm is sensitive to noise in the data. We have found that images of reasonable quality could be produced even with noisy data by increasing the number of measurements, i.e., of electrodes. Of course, this strategy has both practical and intrinsic limits that it would be interesting to study.

3. Another important point to be studied is the optimum resolution achievable for a given number of data. As was shown in Fig. 9, the demand for an excessively high resolution may result in a considerable degradation of the image.

4. The present shape decomposition approach may be extended to three-dimensions, e.g., by using spherical harmonics. This appears to be another fruitful area for research. Some preliminary, very encouraging results have been presented in Ref. [3].

5. One element of the forward problem not included in this study is the modeling of the contact impedance between the conductive medium and the electrodes. In actual experiments, perfect contact with the electrodes may not be an accurate assumption. How a non-zero contact impedance would affect the present results is another point to be examined.

6. Shape decompositions in other than Fourier modes also need to be researched. This flexibility may be of particular value when the general shape of the objects to be searched is known. But one can also explore other orthogonal decompositions, such as Legendre polynomials [20], etc. One of the limitations of expansions such as (4) is that they cannot reproduce certain classes of nearly self-intersecting shapes. In this case, one may use more than one Fourier decompositions for different parts of the boundary—and in this case give up Eqs. (5)—or use, in place of the angle θ, a normalized arc length along the boundary. This approach is not evidently restricted to Fourier decompositions, but can be used for any (orthogonal or non-orthogonal) decomposition.

7. Finally—and most critically—it is necessary to test how the features of this method that have been determined theoretically would stand the test of an actual experiment.

ACKNOWLEDGMENTS

A.P. gratefully acknowledges support from DOE under Grant DE-FG02-89ER14043. D.H. is grateful to ONR for allowing him time to work on this project.

REFERENCES

1. S. L. Ceccio and D. L. George, A review of electrical impedance techniques for the measurement of multiphase flows, *J. Fluids Eng.* **118**, 391 (1996).
2. D. Mewes and D. Schmitz, Tomographic methods for the analysis of flow patterns in steady and transient flows, in *Two-Phase Flow Modelling and Experimentation*, edited by G. P. Celata, P. Di Marco, and R. K. Shah (Edizioni ETS, Pisa, 1999), p. 29.
3. H. N. Oğuz and D. Han, 3-D impedance tomography of high contrast objects, in *Boundary Elements XX*, edited by A. Cassab, M. Chopra, and C. A. Brebbia (Computational Mechanics, Southhampton, 1998), p. 361.
4. C. C. Barber and B. H. Brown, Imaging spatial distributions of resistivity using applied potential tomography, *Electron. Lett.* **19**, 933 (1983).
5. C. C. Barber and B. H. Brown, Applied potential tomography, *J. Phys. E.* **17**, 723 (1984).
6. F. Santosa and M. Vogelius, A backprojection algorithm for electrical impedance imaging, *SIAM J. Appl. Math.* **50**, 216 (1990).
7. R. Guardo, C. Boulay, B. Murray, and M. Bertrand, An experimental study in electrical impedance tomography, *IEEE Trans. Biomed. Eng.* **38**, 617 (1991).
8. T. J. Yorkey, J. G. Webster, and W. J. Tompkins, Comparing reconstruction methods for electrical impedance tomography, *IEEE Trans. Biomed. Eng.* **11**, 843 (1987).
9. F. J. Dickin, R. A. Williams, and M. S. Beck, Determination of composition and motion of multicomponent mixtures in process vessels using electrical impedance tomography. I. Principles and process engineering applications, *Chem. Eng. Sci.* **48**, 1883 (1993).

10. D. L. George, S. L. Ceccio, J. R. Torczynski, K. A. Shollenberger, and T. J. O'Hern, Validation of electrical impedance tomography for measurement of material distribution in two-phase flows, *Int. J. Multiphase Flow*, in press.
11. N. Reinecke and D. Mewes, Multielectrode capacitance sensors for the visualization of transient two-phase flows, *Exp. Thermal Fluid Sci.* **15**, 253 (1997).
12. M. A. Jaswon and G. T. Symm, *Integral Equation Methods in Potential Theory and Elastostatics* (Academic Press, San Diego, 1977).
13. C. Pozrikidis, *Boundary Integral and Singularity Methods for Linearized Viscous Flow* (Cambridge Univ. Press, Cambridge, UK, 1992).
14. W. H. Press, W. T. Vetterling, S. A. Teukolsky, and B. P. Flannery, *Numerical Recipes in FORTRAN*, 2nd ed. (Cambridge Univ. Press, Cambridge, UK, 1992).
15. K. Cheng, D. Isaacson, J. C. Newell, and D. G. Gisser, Electrode models for electric current computed tomography, *IEEE Trans. Biomed. Eng.* **36**, 918 (1989).
16. K. Paulson, W. Breckon, and M. Pidcock, Electrode modeling in electrical impedance tomography, *SIAM J. Appl. Math.* **52**, 1012 (1992).
17. M. Murai and Y. Kagawa, Electrical impedance computed tomography based on a finite element model, *IEEE Trans. Biomed. Eng.* **32**, 177 (1985).
18. M. Murai and Y. Kagawa, Boundary element iterative technique for determining the interface boundary between two Laplace domains—A basic study of impedance plethysmography as an inverse problem, *Int. J. Numer. Methods Eng.* **23**, 35 (1986).
19. O. C. Jones, J. T. Lin, H. Shu, L. Ovacik, and Y. He, Impedance imaging relative to binary mixtures, in *Liquid-Solid Flows*, edited by M. C. Roco, C. T. Crowe, D. D. Joseph, and E. E. Michaelides (ASME, New York, 1994), Vol. FED-189, p. 91.
20. R. Duraiswami, G. L. Chahine, and K. Sarkar, Efficient 2D and 3D electrical impedance tomography using boundary element methods, *Chem. Eng. Sci.* **52**, 2185 (1997).